Supporting Information for

Sulfur-Containing Block Polymers from Ring-Opening Copolymerisation: Coordinative Encapsulants for Transition Metals

Table of contents

Methods

Solvents and reagents were obtained from commercial sources. These have been used without any further purification unless otherwise stated. NMR spectra were recorded by using a JEOL JNM-ECA 400II, JOEL ECZ600 and BRUKER AVANCE500 spectrometer. ^{1}H, $^{13}C\{^{1}H\}$, ^{19}F and $^{31}P\{^{1}H\}$ chemical shifts are referenced to the residual proton resonance of the deuterated solvents.

Oxetane was dried first via distillation over calcium hydride, followed by distillation over sodium and stored in an argon-filled glovebox. Isothiocyanates were dried via distillation over calcium hydride and stored in an argon-filled glovebox. The catalysts LCrRb and phthalic thioanhydride (PTA) were synthesized according to literature procedures.[1,2] mPEG-b-(OX-co-PhNCS) was obtained according to our previous report.[3]

For Cryo-TEM measurements, perforated carbon film-covered microscopical 200 mesh grids (R1/4 batch of Quantifoil) were employed. The grids were cleaned with chloroform and hydrophilized through a 60-second glow discharge at 10 mA in a Safematic CCU-010 device. Subsequently, 4 µl aliquots of the sample solution were applied to the grids. The samples underwent vitrification through automated blotting and rapid freezing using an FEI Vitrobot Mark IV with liquid ethane as a cryogenic agent. The vitrified specimens were then transferred to the autoloader of an FEI TALOS ARCTICA electron microscope. This microscope, equipped with a high-brightness field-emission gun (XFEG), operated at an acceleration voltage of 200 kV. Micrographs capturing detailed specimen features were acquired using an FEI Falcon 3 direct electron detector with a 100 µm objective aperture. To obtain spatial information of the samples, tomograms were recorded on the TALOS® ARCTICA transmission electron microscope (ThermoFisher Scientific Inc., Waltham (MA), USA) at 200 kV. For this purpose, single axis tilt series (±64° in 2° tilt angle increments) were acquired with a FEI Falcon 3EC 4k×4k direct electron detector at 28 K primary magnification with a total dose lower than 120 e-/Å2. Reconstruction of the tomograms was performed with binned data (binning factor 2) using ThermoFisher Inspect3D software, version 3.1.0. The 3D voltex presentation was prepared using Amira, Version 6.2 (ThermoFisher Scientific Inc., Waltham (MA), USA).

DSC TA 4000 or Mettler Toledo STAR System DSC 3+ was used for the DSC experiments under N_2 flow. The first heating is up to T_m + 10ºC to avoid degradation of the polymer and isotherm for 3 min to erase the thermal history, after the cooling up to -50ºC, and the second heating up to T_m + 10ºC. All the scans were made at 10 ºC min^{-1}. TGA for all polymers was measured using a Netzsch TG 209 or a Mettler Toledo STAR System TGA/DSC 3+ (heating rate 10 K/min).

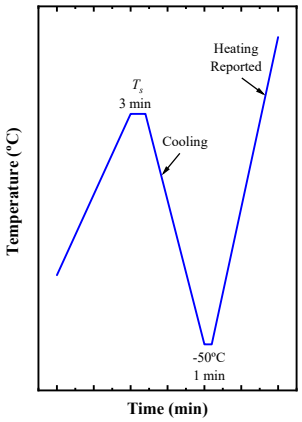

Figure S1: Procedure for SN experiments.

Since the semi-crystalline polymers do not crystallize completely from a fully molten state, a self-nucleation (SN) technique was used as it allows us to study the crystallization in polymers that crystallize very slowly, accelerating the primary nucleation. Figure S1 shows the procedure used for the SN, for all the polymers different T_s were selected, the lowest T_s is exactly at the peak of the melting temperature, the highest T_s is exactly where the melting peak ends, and finally an intermediate T_s between the two T_s mentioned. For the study of each T_s a fresh sample was used, so the heat treatment of the sample is that of the synthesis.

DLS data were obtained using a Malvern Zetasizer Ultra equipped with a 10 mW He-Ne laser operating at a wavelength of 632.8 nm, and the analysis was conducted using the ZS Xplorer software. Fluorescence spectra were recorded using a Fluorescence FL 6500 instrument, and UV/Vis measurements were conducted using a UV-vis Lambda 365 spectrometer.

The determination of the molecular weight and polydispersity of the polymers was conducted using a Waters 1515 gel permeation chromatography (GPC) instrument, which was equipped with two linear PLgel columns (Mixed-C), a guard column, and a differential refractive index detector. Tetrahydrofuran was employed as the eluent at a flow rate of 1.0 mL/min, and the analysis was carried out at 30 °C. Column calibration was achieved using narrow polystyrene standards. Prior to analysis, each polymer sample was dissolved in HPLC-grade THF at a concentration of 1 mg/mL and subsequently filtered through a 0.20 µm porous filter frit.

Blockpolymer Synthesis and Characterization

General Polymerization Procedure

LCrRb (1 eq.), m-PEG (5 kDa, 20 eq.), (oxetane, 1200 eq.) and the iso thiocyanate or PTA (1000 eq.) were added to an oven-dried screw-cap vial with an oven-dried stirrer bar inside an argon filled glovebox. The loaded vials were then placed in a preheated (80 °C) aluminium block. After full monomer conversion as determined by NMR aliquot analysis, the crude mixture was dissolved in about 5 ml dichloromethane and precipitated by addition into about 50 ml methanol. In some cases, this was followed by precipitation from dichloromethane/pentane. The precipitated polymer was isolated by centrifugation and dried under vacuum.

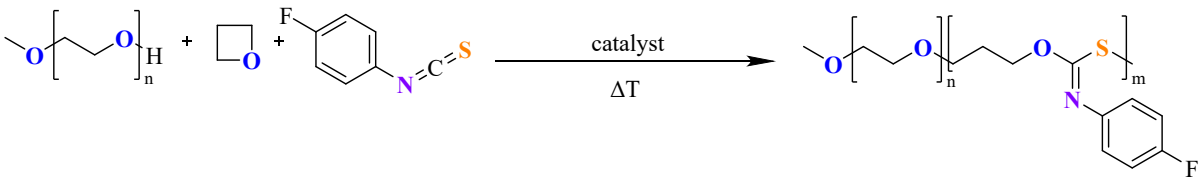

Scheme S 1:Synthesis of mPEG-b-(OX-co-^{F}PhNCS).

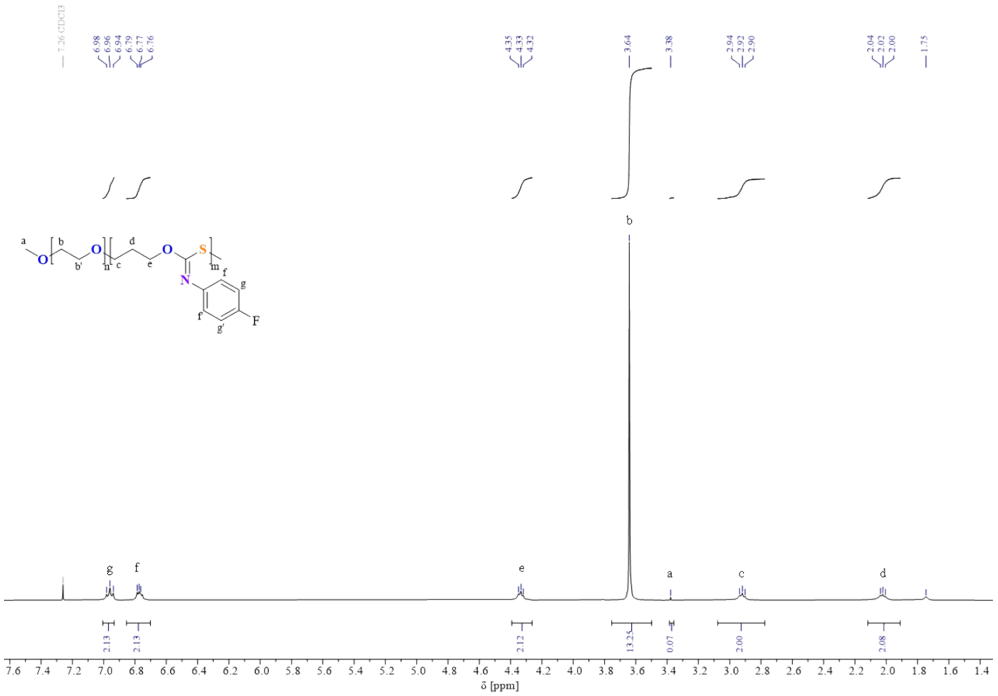

Figure S2: ^{1}H NMR spectrum (400 MHz, $CDCl_3$, 25°C) of mPEG-*b*-(OX-*co*-^{F}PhNCS).

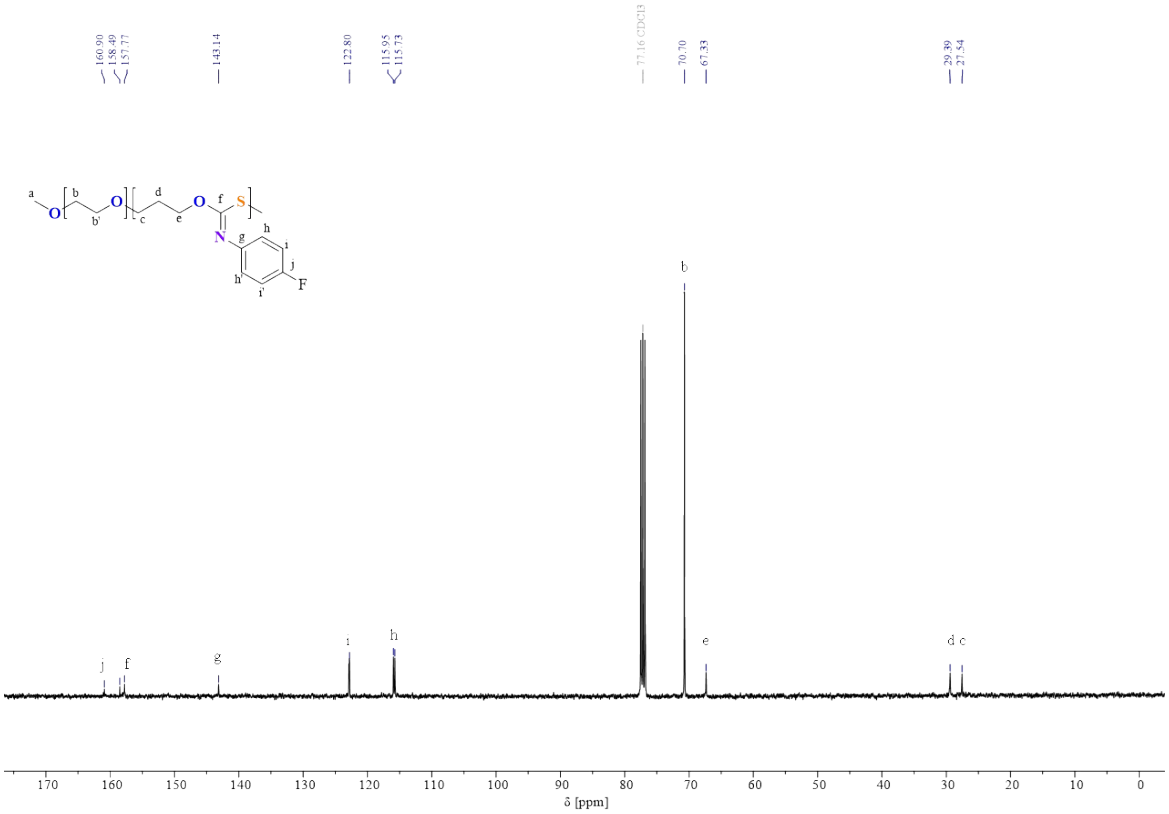

Figure S3: ^{13}C NMR spectrum (126 MHz, $CDCl_3$, 25°C) of mPEG-*b*-(OX-*co*-^{F}PhNCS).

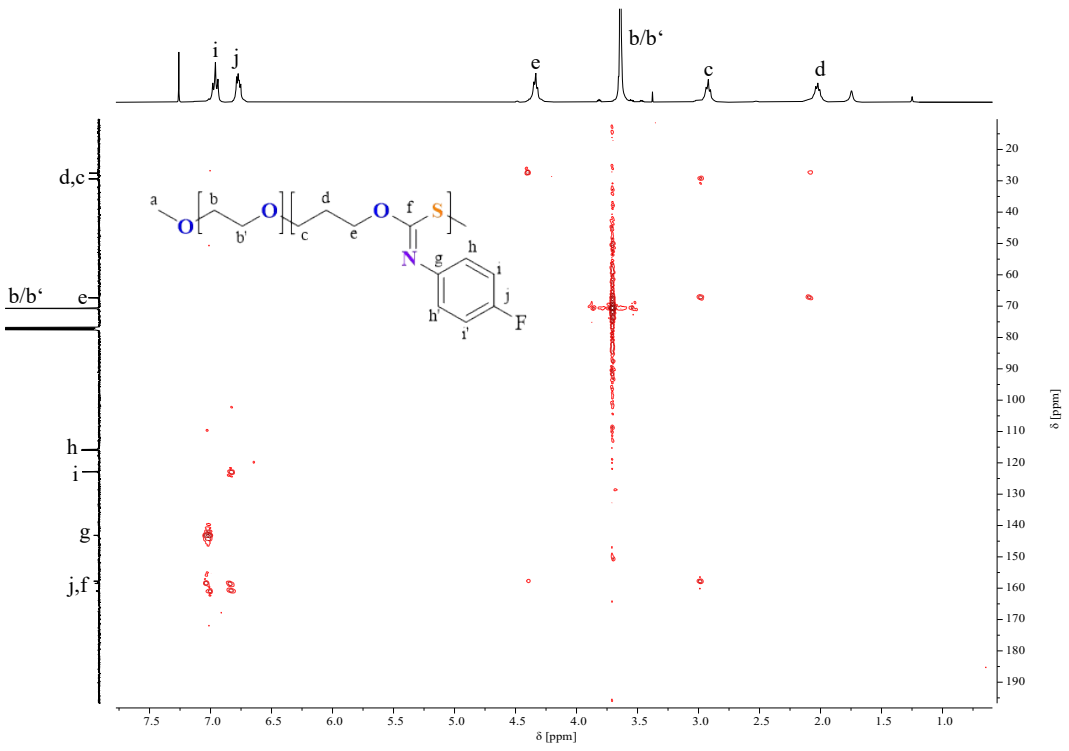

Figure S4: ^{1}H-^{13}C HMBC NMR spectrum ($CDCl_3$, 25°C) of mPEG-*b*-(OX-*co*-^{F}PhNCS).

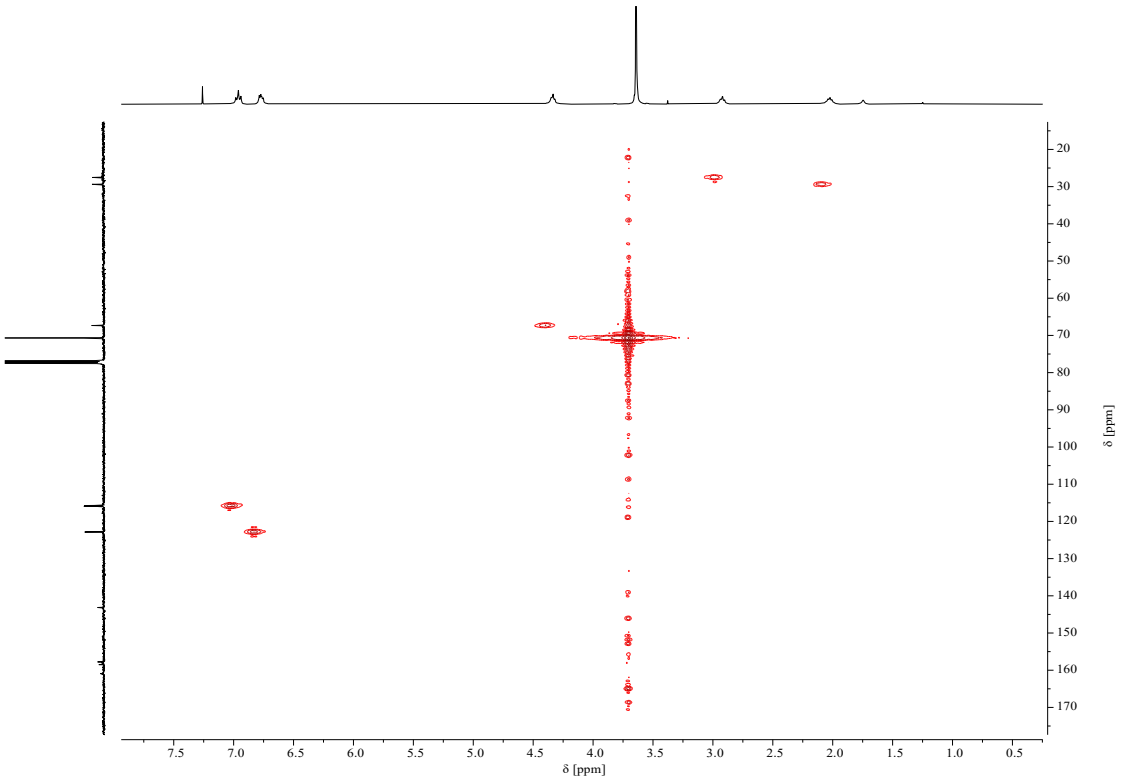

Figure S5: ^{1}H-^{13}C HMQC NMR spectrum ($CDCl_3$, 25°C) of mPEG-*b*-(OX-*co*-^{F}PhNCS).

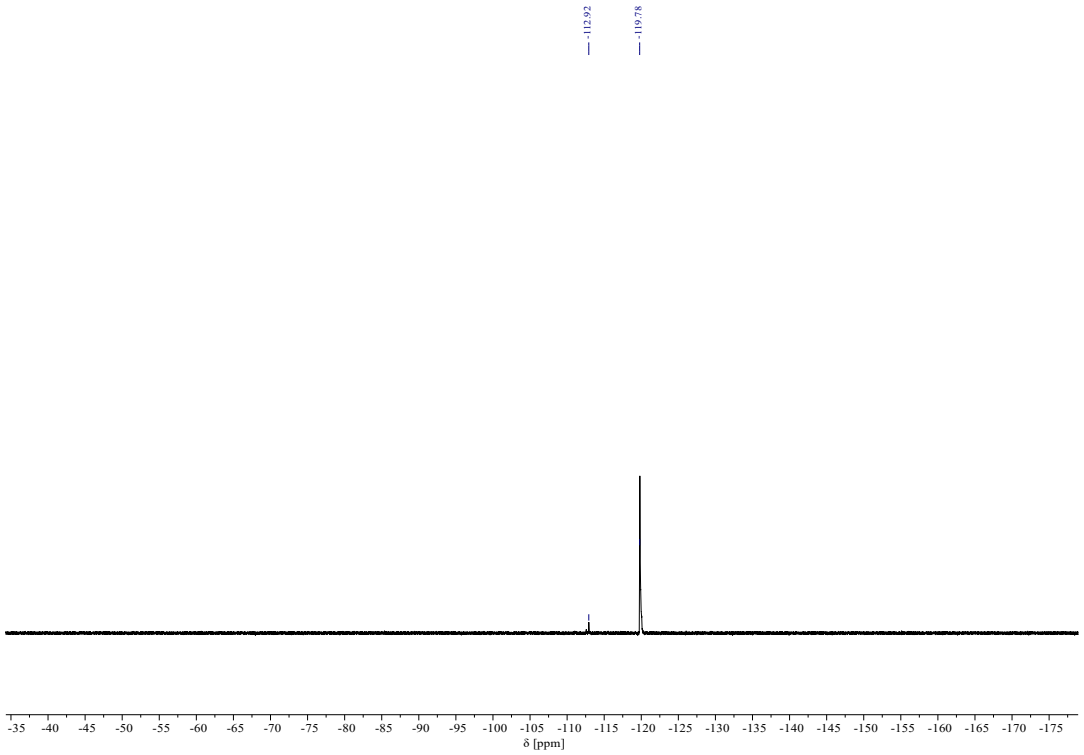

Figure S6: ^{19}F NMR spectrum (126 MHz, $CDCl_3$, 25°C) of mPEG-*b*-(OX-*co*-^{F}PhNCS). Signal at -113 ppm attributed to trace OSN links.[3]

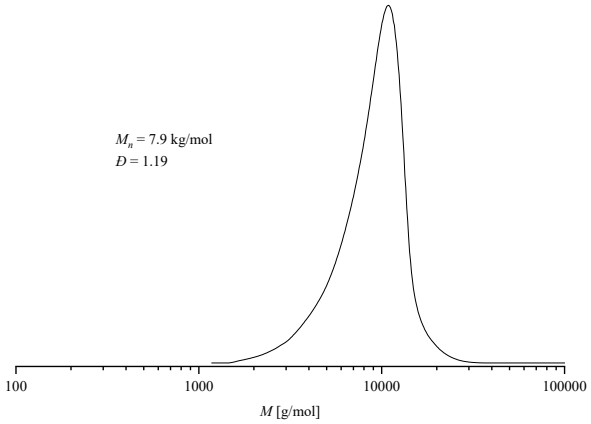

Figure S7: GPC traces of mPEG-*b*-(OX-*co*-^{F}PhNCS).

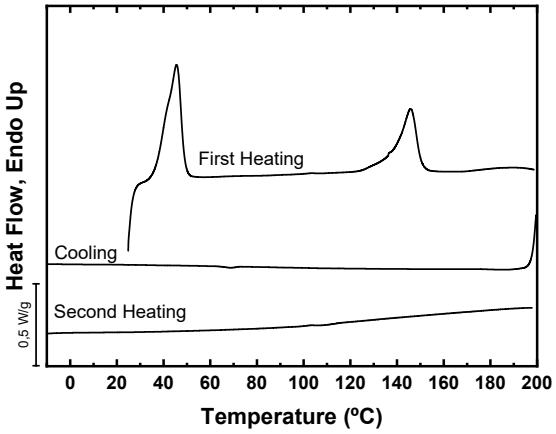

Figure S8: DSC data of mPEG-*b*-(OX-*co*-^{F}PhNCS).

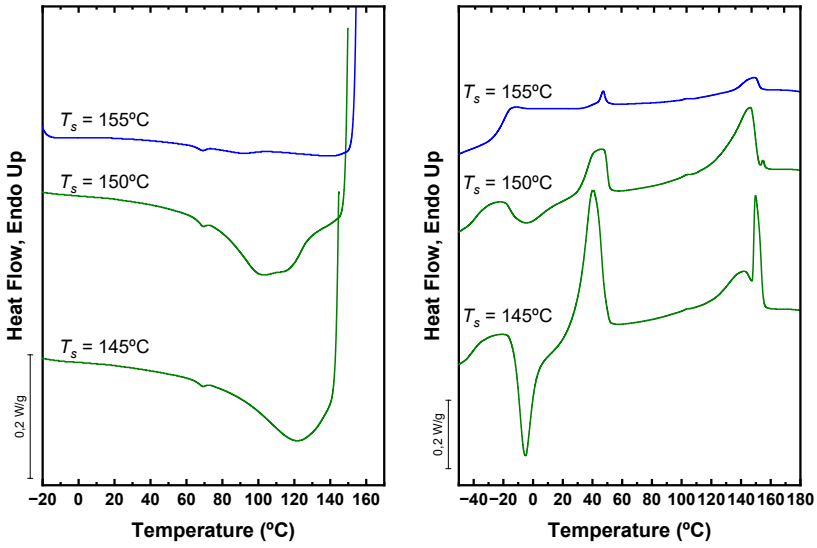

Figure S9: SN experiments for mPEG-*b*-(OX-*co*-^{F}PhNCS).

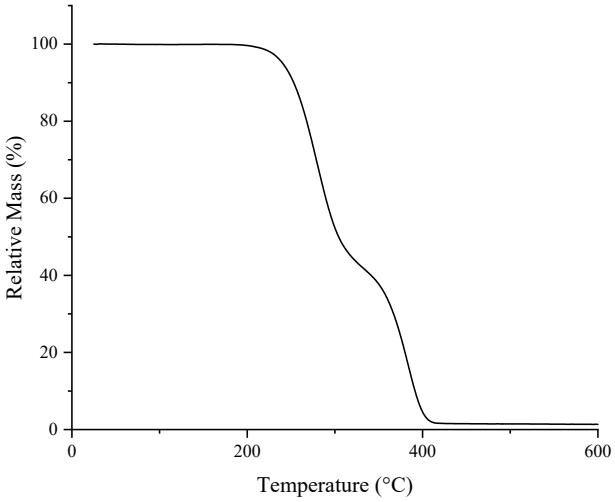

Figure S10: TGA data for mPEG-*b*-(OX-*co*-^{F}PhNCS).

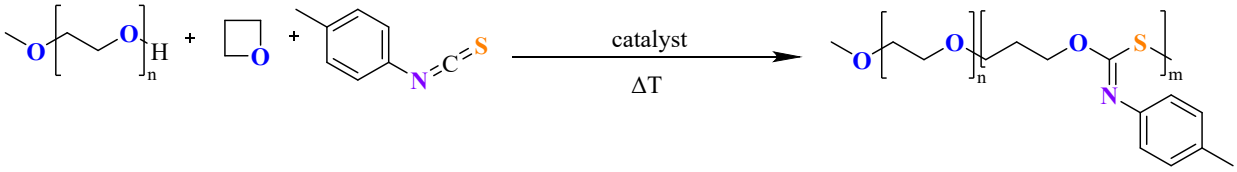

Scheme S2: Synthesis of mPEG-*b*-(OX-*co*-^{Me}PhNCS).

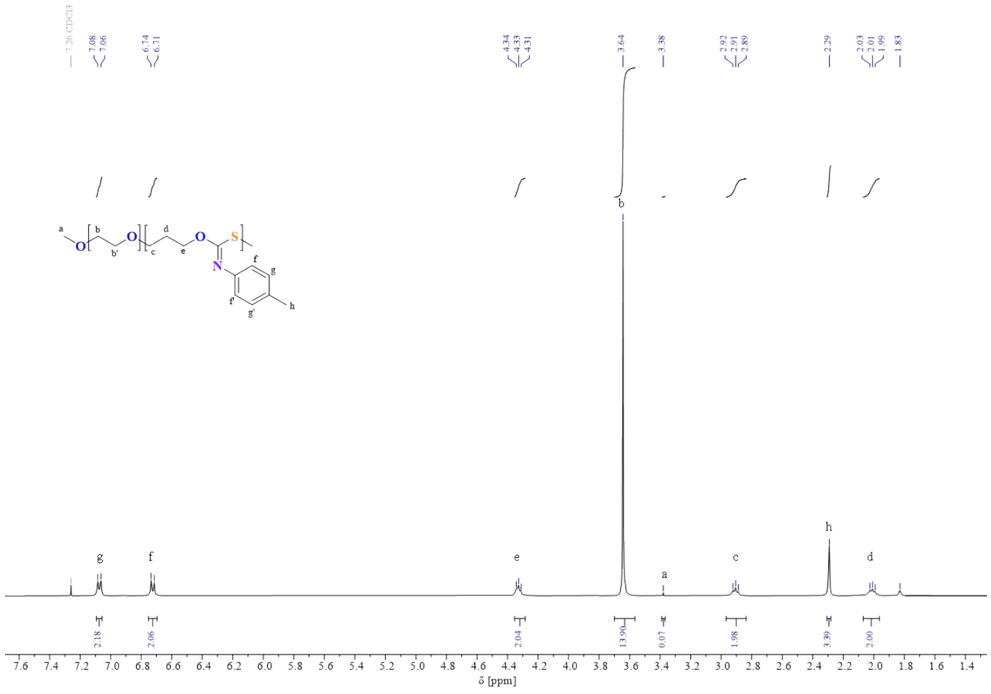

Figure S11: ^{1}H NMR spectrum (400 MHz, $CDCl_3$, 25°C) of mPEG-*b*-(OX-*co*-^{Me}PhNCS).

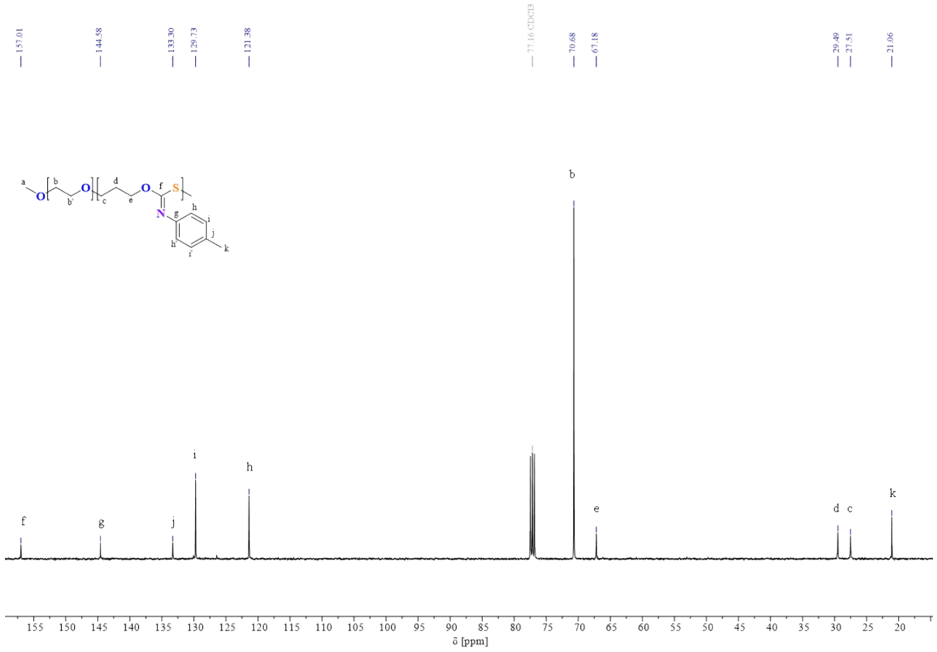

Figure S12: ^{13}C NMR spectrum (126 MHz, $CDCl_3$, 25°C) of mPEG-*b*-(OX-*co*-^{Me}PhNCS).

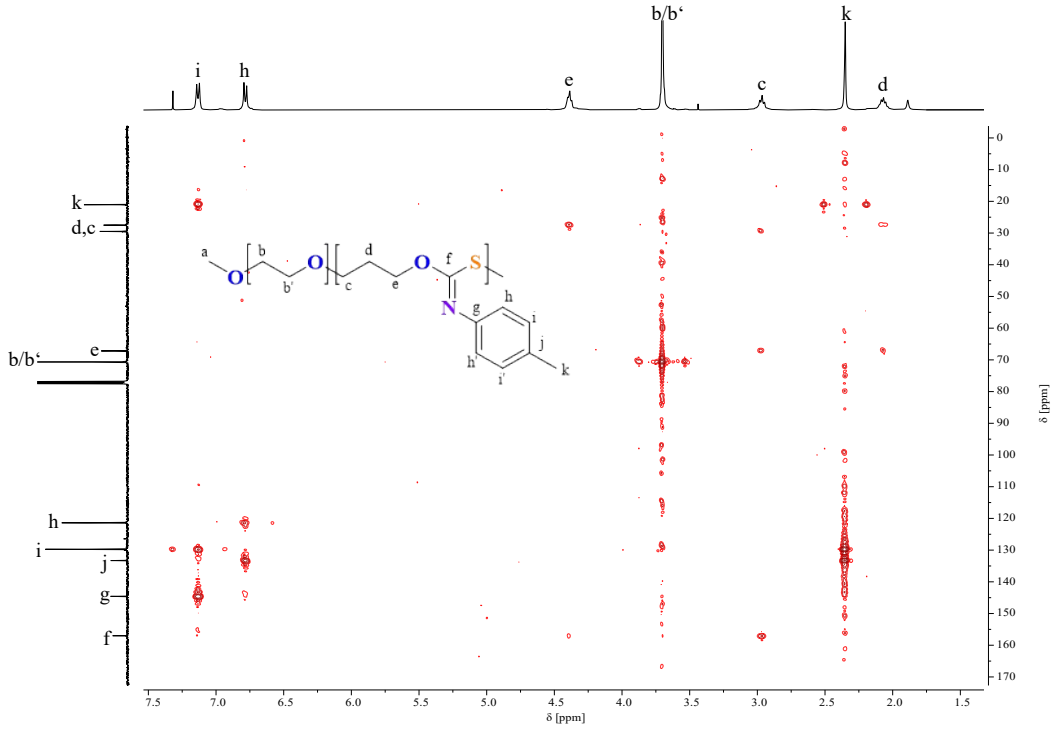

Figure S13: ^{1}H-^{13}C HMBC NMR spectrum ($CDCl_3$, 25°C) of mPEG-*b*-(OX-*co*-^{Me}PhNCS).

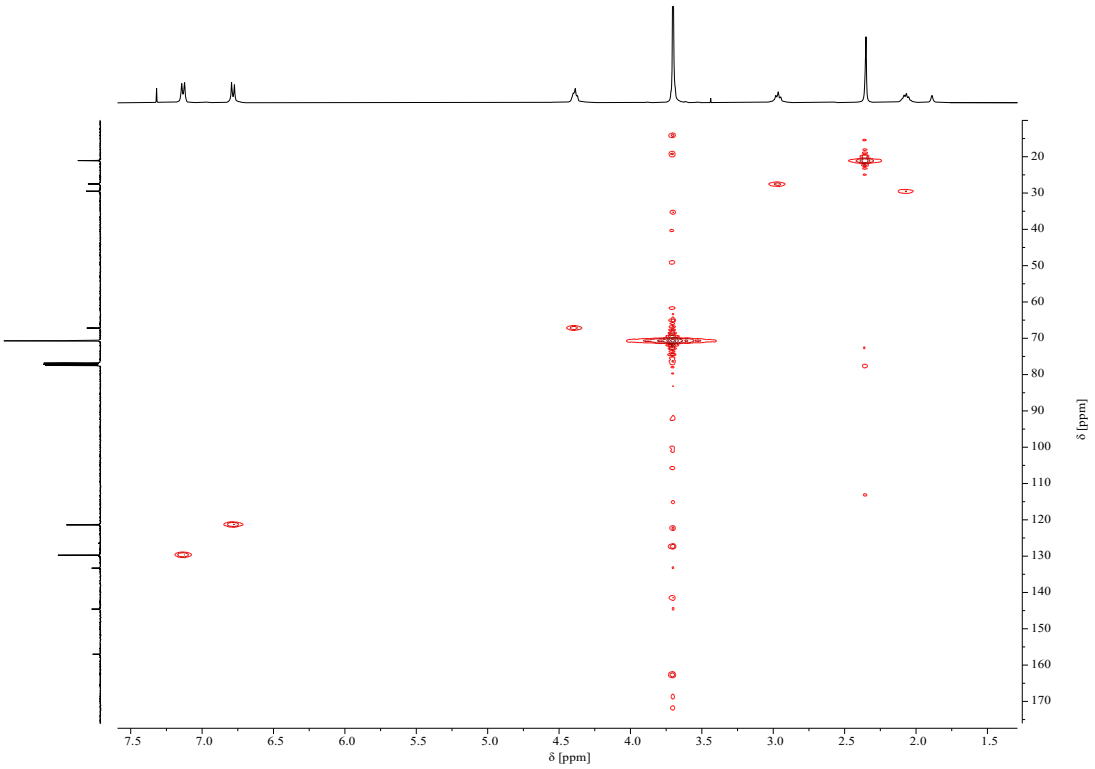

Figure S14: ^{1}H-^{13}C HMQC NMR spectrum ($CDCl_3$, 25°C) of mPEG-*b*-(OX-*co*-^{Me}PhNCS).

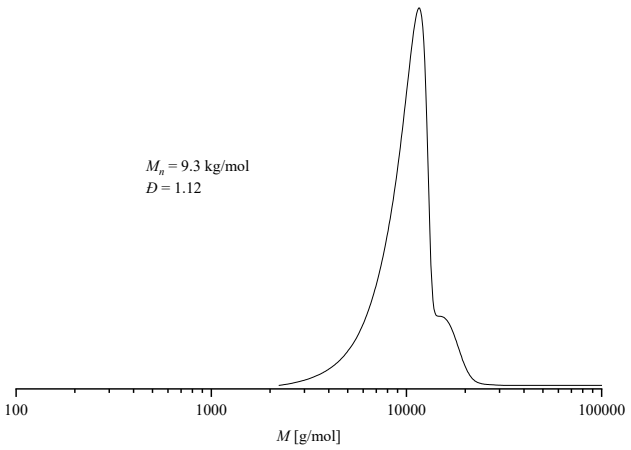

Figure S15: GPC traces of mPEG-*b*-(OX-*co*-^{Me}PhNCS).

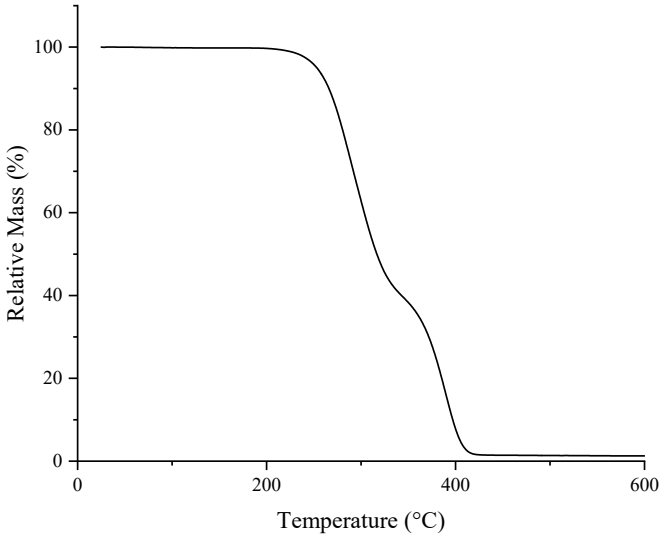

Figure S16: TGA data for mPEG-*b*-(OX-*co*-^{Me}PhNCS).

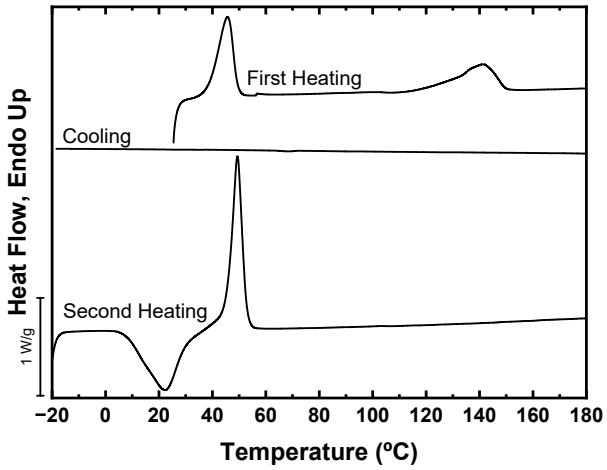

Figure S17: DSC data of mPEG-*b*-(OX-*co*-^{Me}PhNCS).

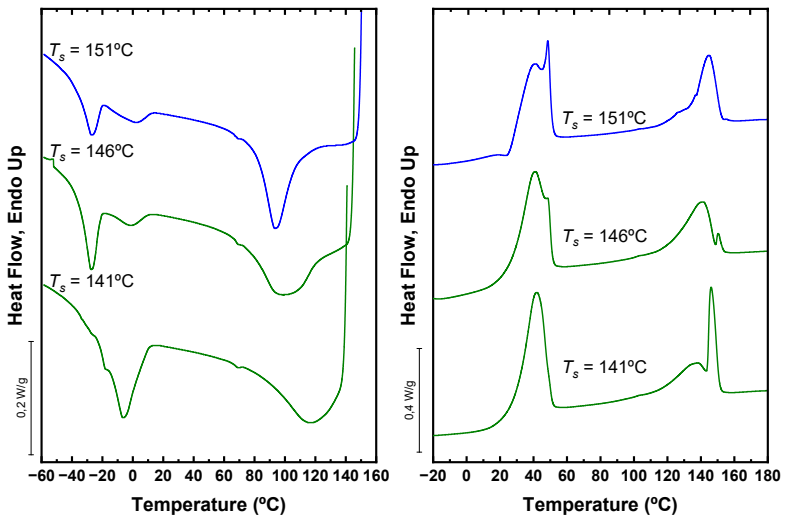

Figure S18: SN experiments for mPEG-*b*-(OX-*co*-^{Me}PhNCS).

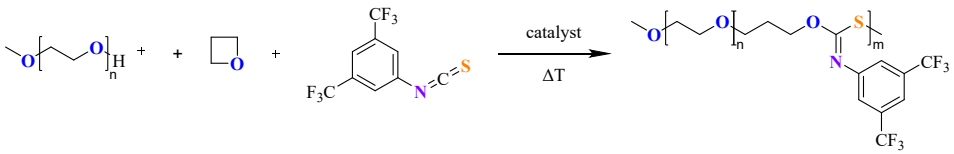

Scheme S3: Synthesis of mPEG-*b*-(OX-*co*-$^{(CF3)2}$PhNCS).

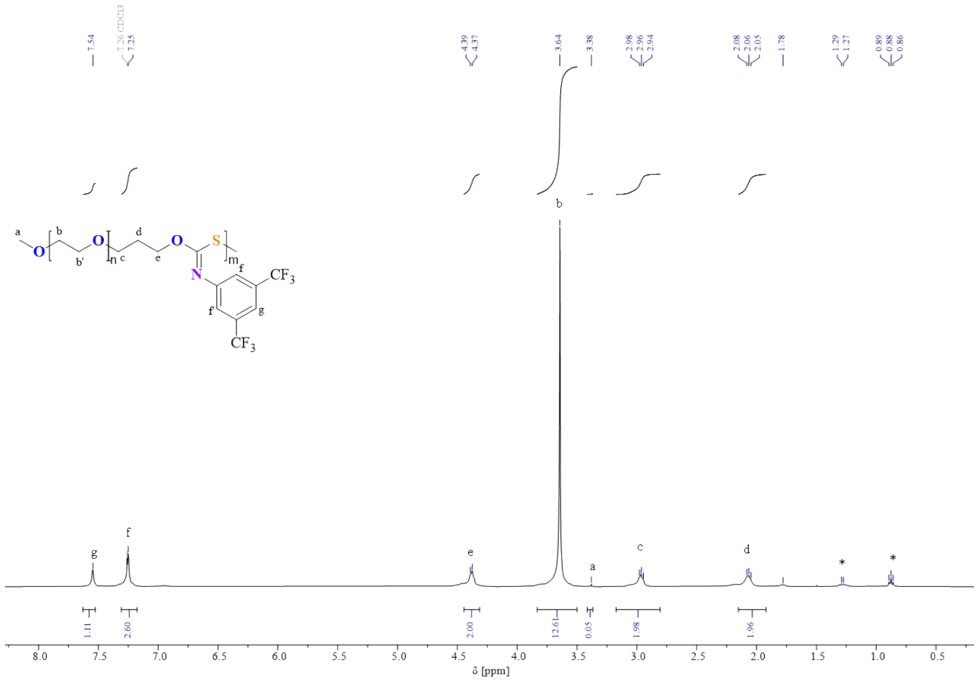

Figure S19: ^{1}H NMR spectrum (400 MHz, $CDCl_3$, 25°C) of mPEG-b-(OX-co-$^{(CF3)2}$PhNCS) (* = residual pentane).

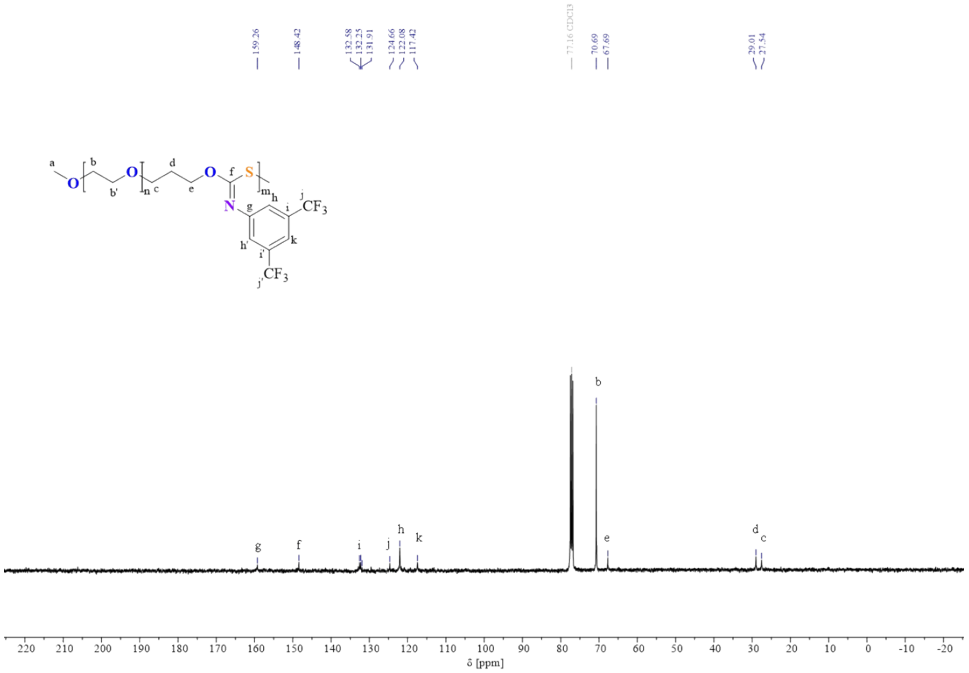

Figure S20: ^{13}C NMR spectrum (126 MHz, $CDCl_3$, 25°C) of mPEG-b-(OX-co-$^{(CF3)2}$PhNCS).

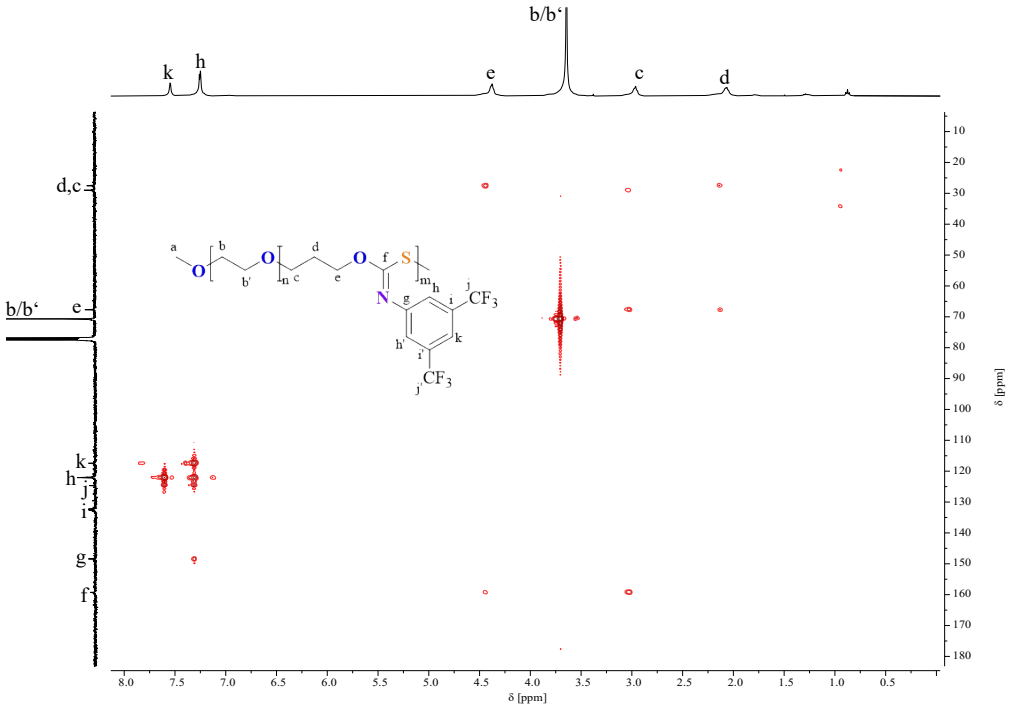

Figure S21: ^{1}H-^{13}C HMBC NMR spectrum ($CDCl_3$, 25°C) of mPEG-*b*-(OX-*co*-$^{(CF3)2}$PhNCS).

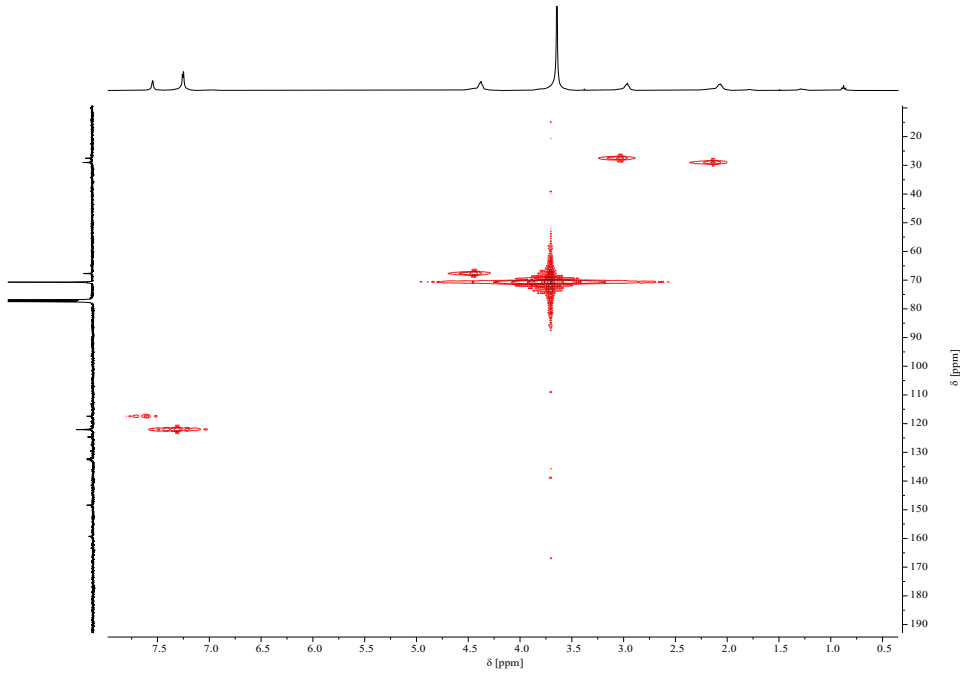

Figure S22: ^{1}H-^{13}C HMQC NMR spectrum ($CDCl_3$, 25°C) of mPEG-*b*-(OX-*co*-$^{(CF3)2}$PhNCS).

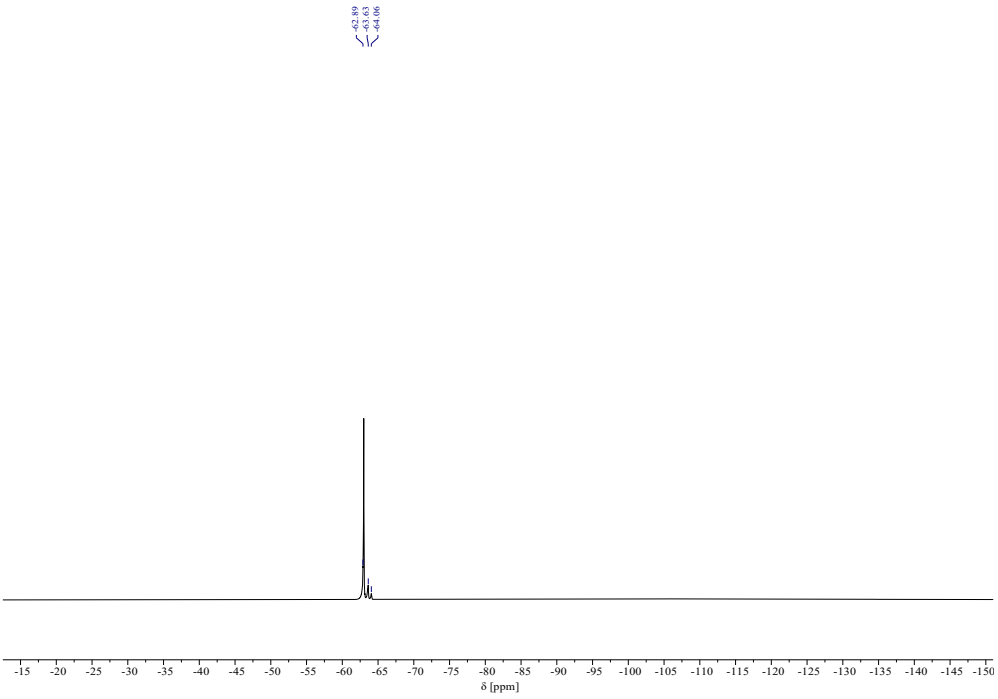

Figure S23: ^{19}F NMR spectrum (126 MHz, $CDCl_3$, 25°C) of mPEG-*b*-(OX-*co*-$^{(CF3)2}$PhNCS). Additional minor resonances attributed to OSN links.[3]

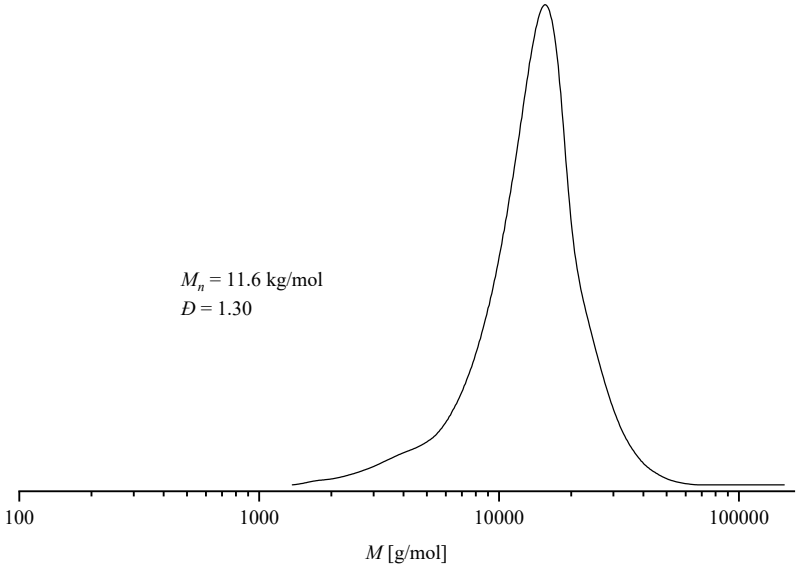

Figure S24: GPC traces of mPEG-*b*-(OX-*co*-$^{(CF3)2}$PhNCS).

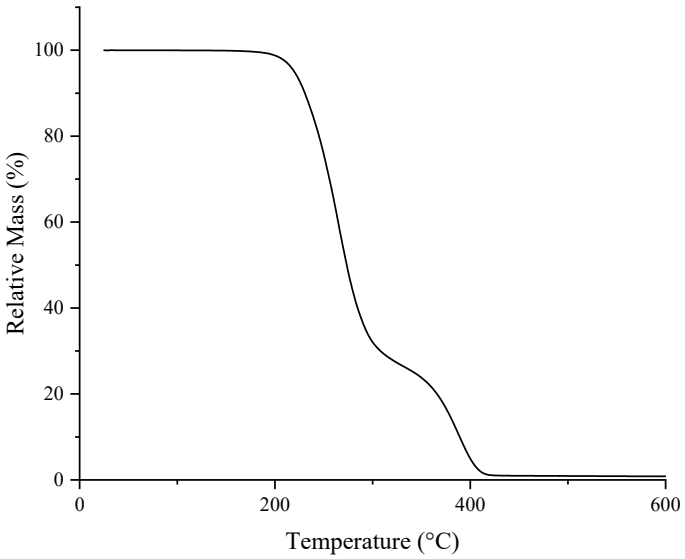

Figure S25**:** TGA data for mPEG-*b*-(OX-*co*-$^{(CF3)2}$PhNCS).

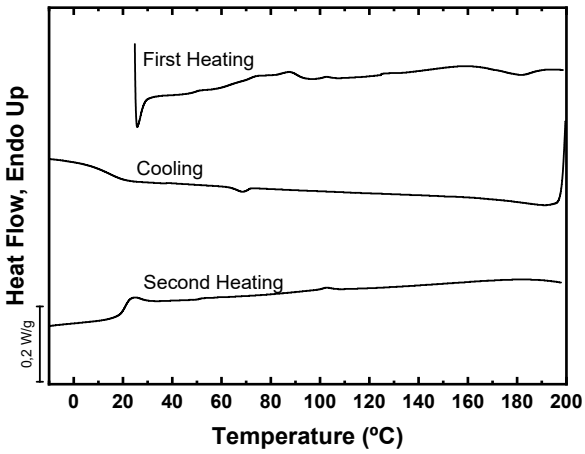

Figure S26: DSC data of mPEG-*b*-(OX-*co*-$^{(CF3)2}$PhNCS).

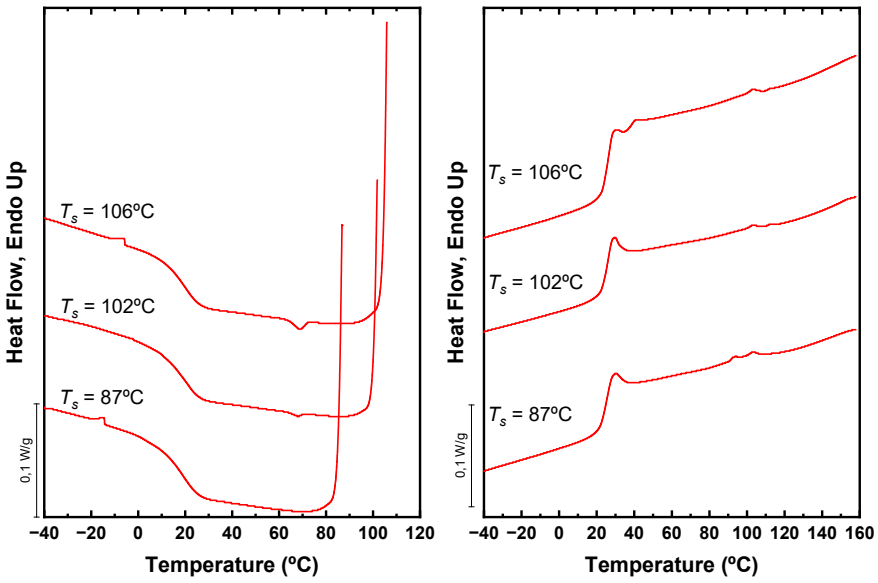

Figure S27: SN experiments for mPEG-*b*-(OX-*co*-$^{(CF3)2}$PhNCS).

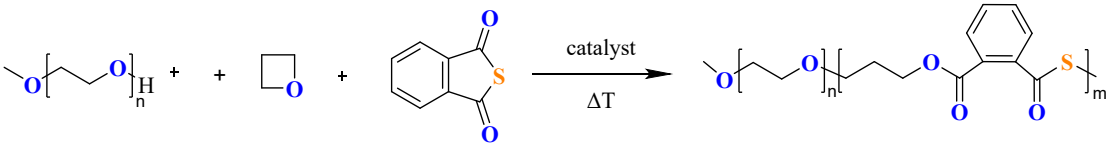

Scheme S4: Synthesis of mPEG-*b*-(OX-*co*-PTA).

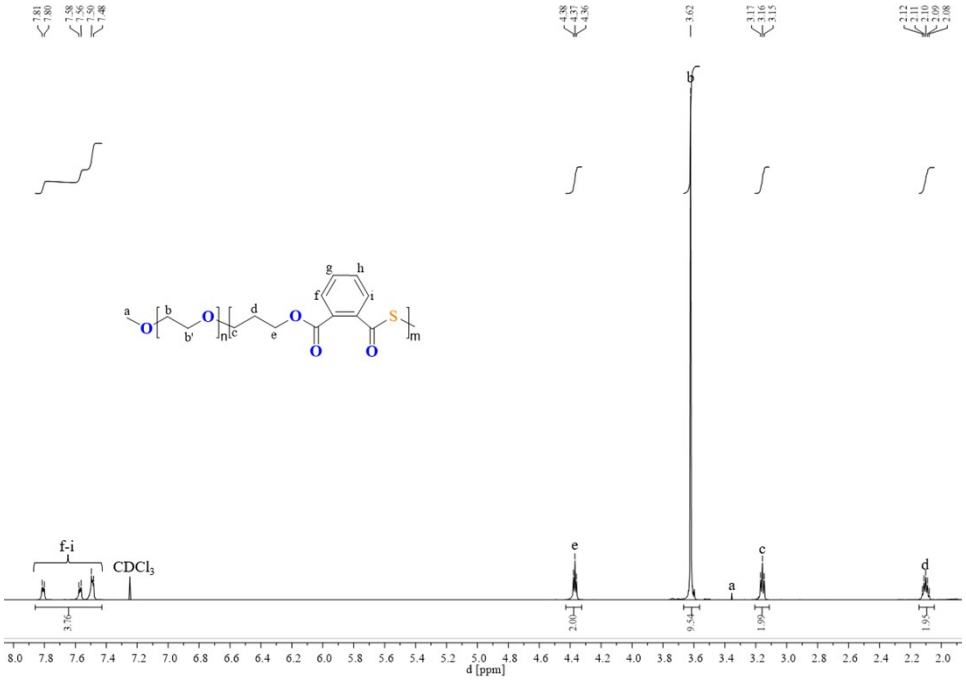

Figure S28: ^{1}H NMR spectrum (400 MHz, $CDCl_3$, 25°C) of mPEG-*b*-(OX-*co*-PTA).

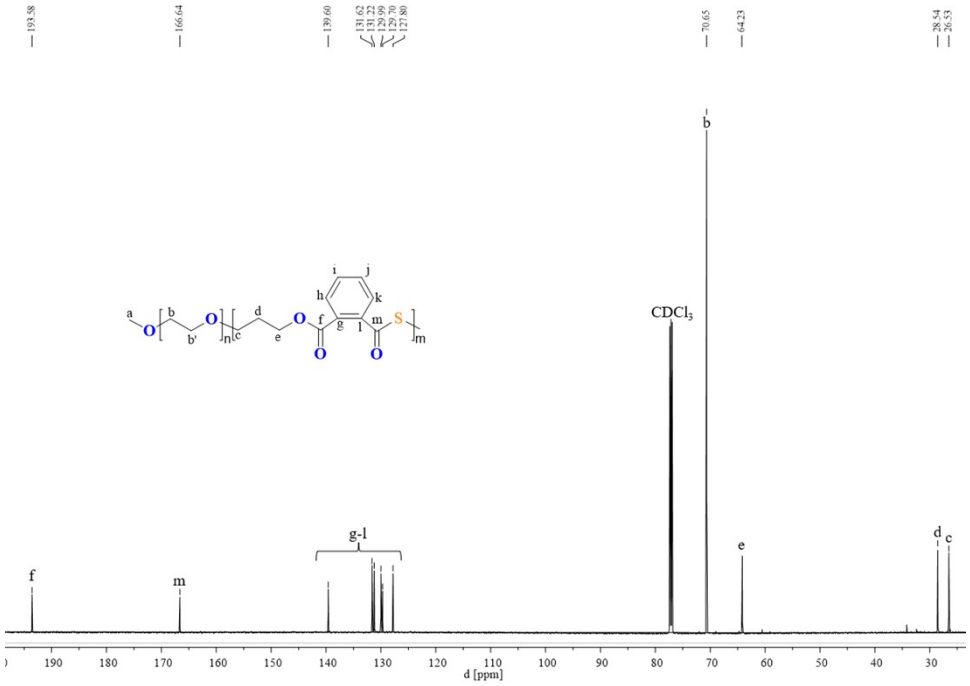

Figure S29: ^{13}C NMR spectrum (126 MHz, $CDCl_3$, 25°C) of mPEG-*b*-(OX-*co*-PTA).

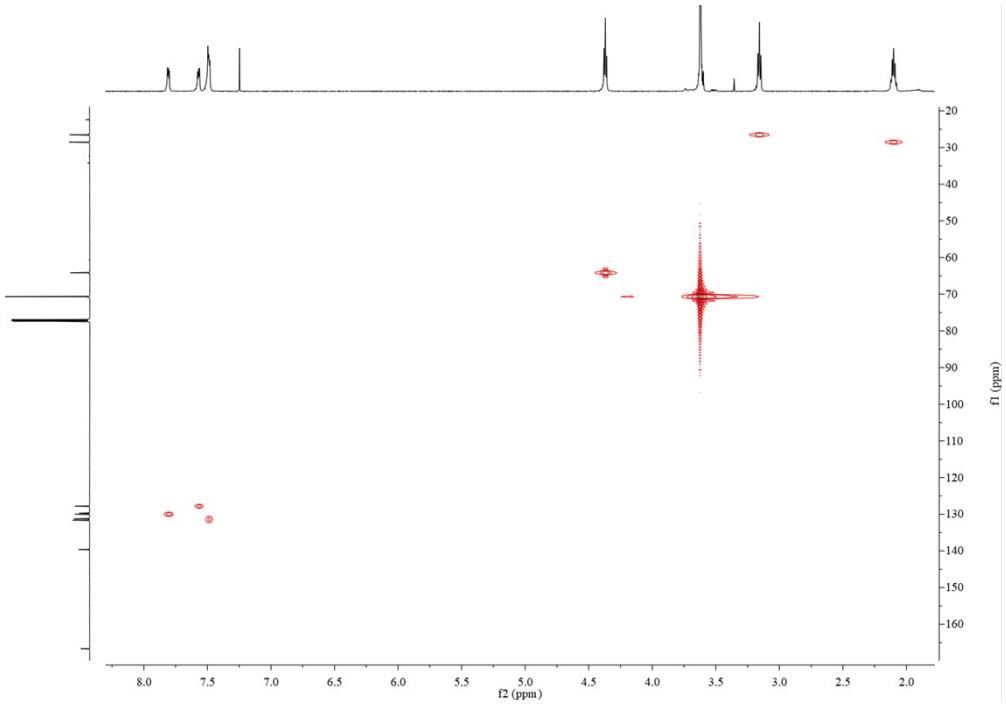

Figure S30: ^{1}H-^{13}C HMQC NMR spectrum ($CDCl_3$, 25°C) of mPEG-*b*-(OX-*co*-PTA).

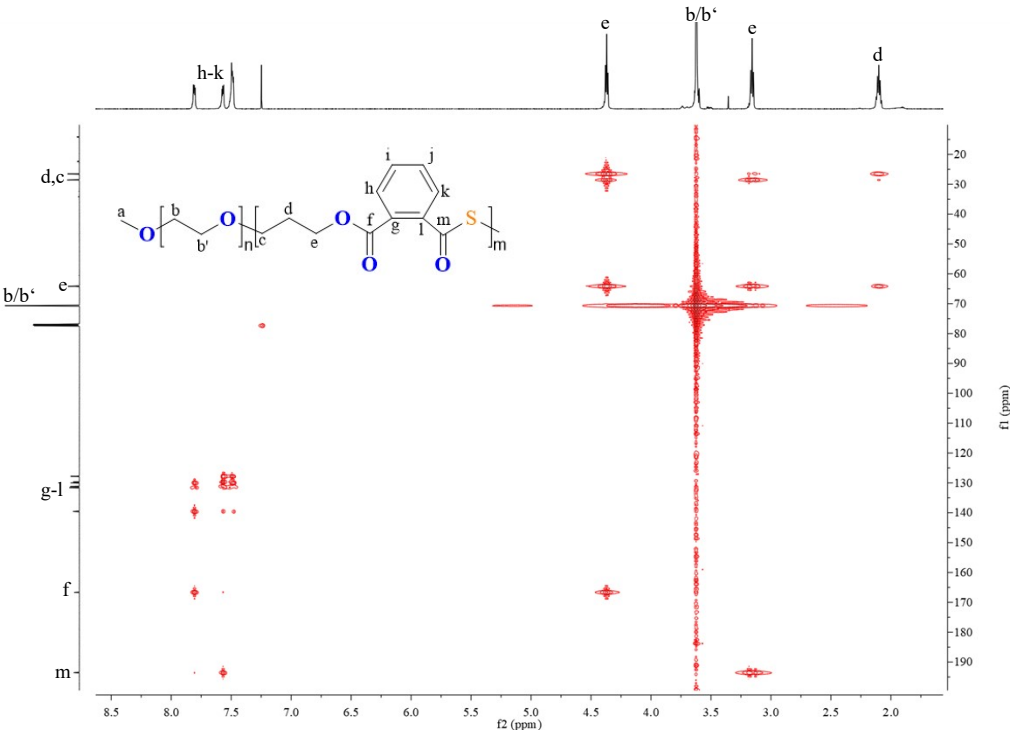

Figure S31: ^{1}H-^{13}C HMBC NMR spectrum ($CDCl_3$, 25°C) of mPEG-*b*-(OX-*co*-PTA).

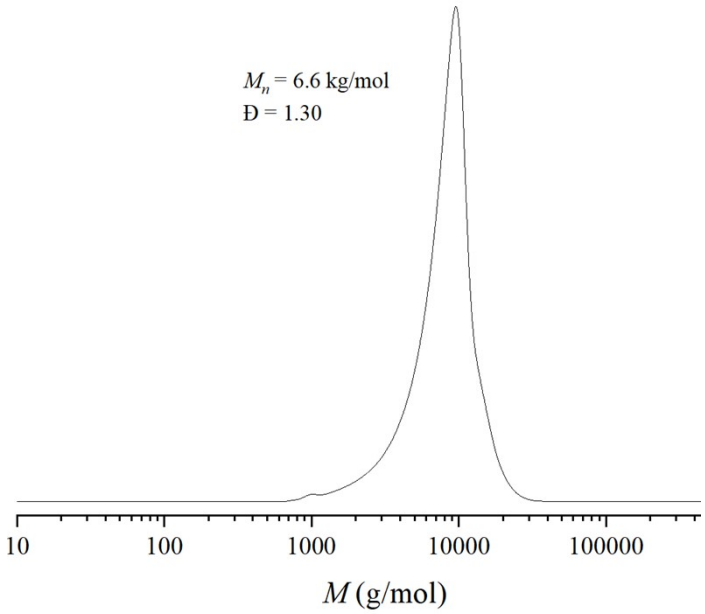

Figure S32: GPC traces of mPEG-b-(OX-co-PTA).

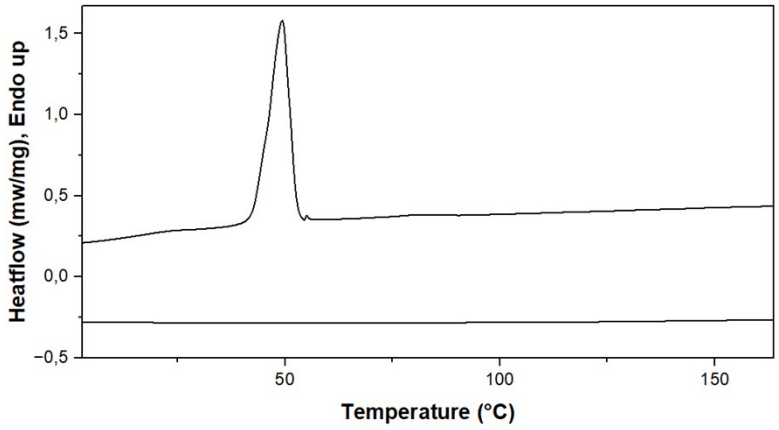

Figure S33: DSC data of mPEG-b-(OX-co- PTA). (top) First cooling, (bottom) second heating.

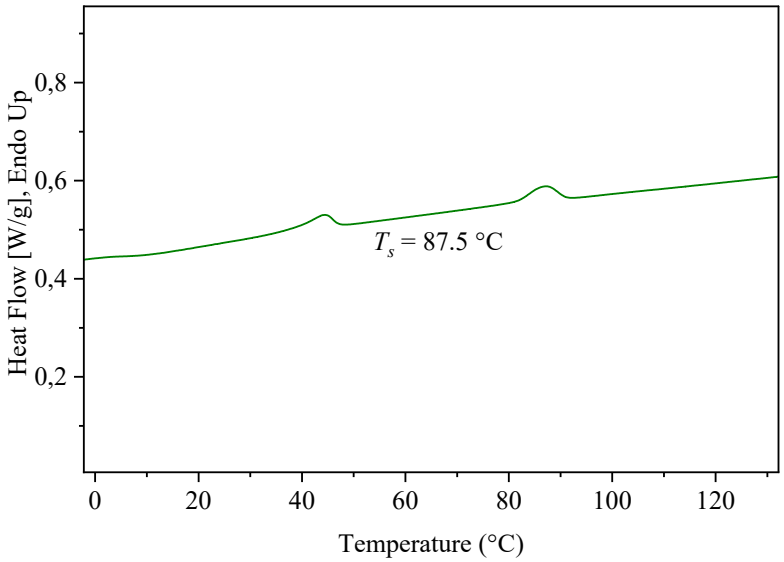

Figure S34: SN experiments for mPEG-*b*-(OX-*co*-PTA).

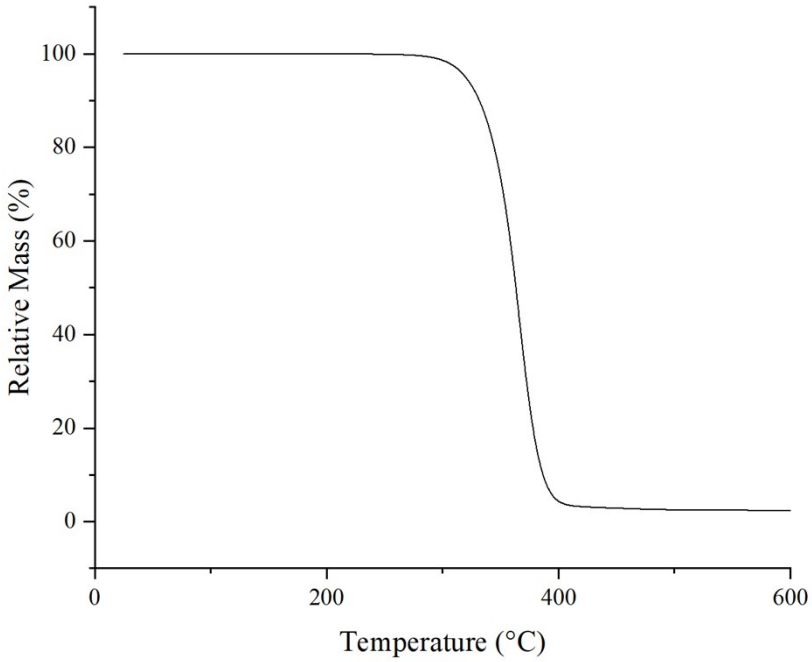

Figure S35: TGA data of mPEG-*b*-(OX-*co*-PTA).

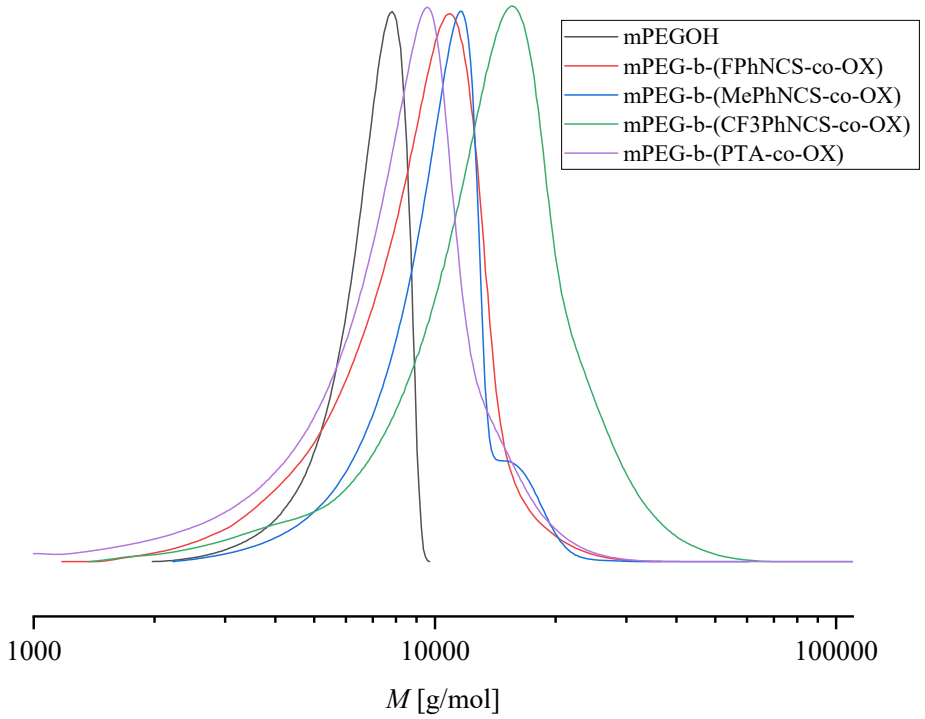

Figure S36: Comparison of GPC data of block polymers with mPEGOH macroinitiator.

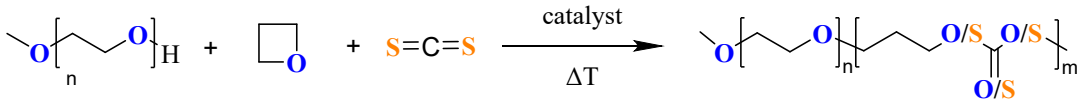

Scheme S5: Synthesis of mPEG-*b*-(OX-*co*-PTA).

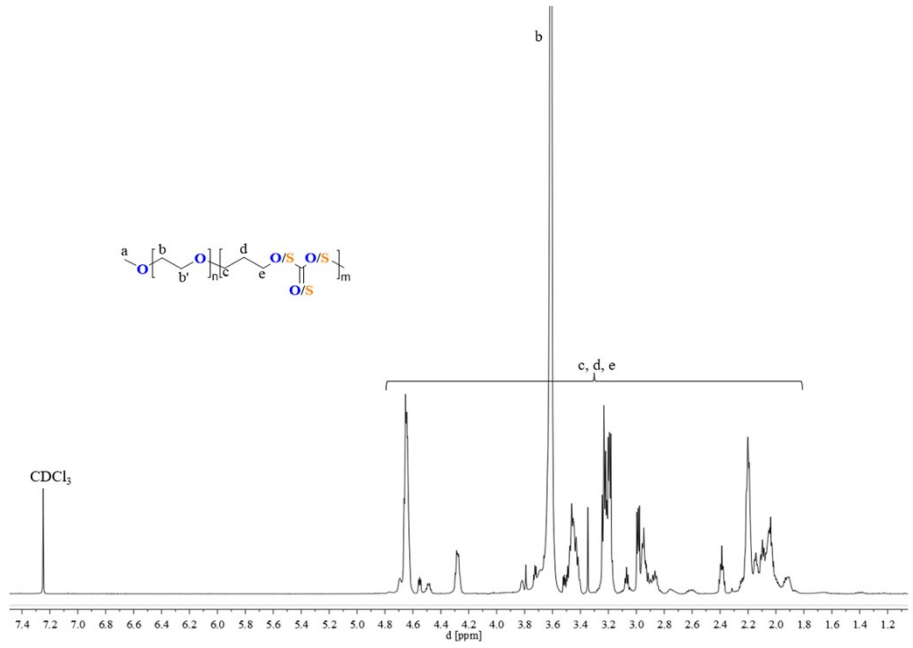

Figure S37: ^{1}H NMR spectrum (400 MHz, $CDCl_3$, 25°C) of mPEG-*b*-(OX-*co*-CS_2).

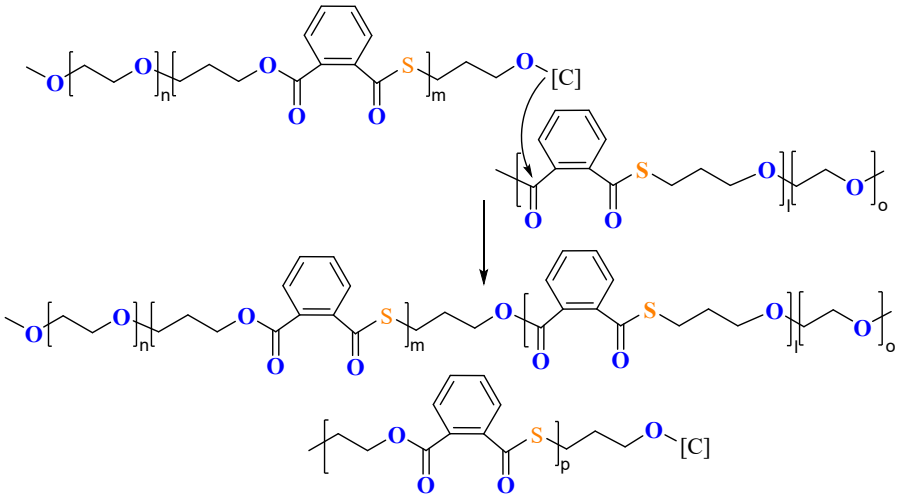

Scheme S6: Example side reaction pathway.

Self-assembly

General procedure: The aggregates were formed by nanoprecipitation. For this purpose, 10 mg of the block polymers were dissolved in 1,4-dioxane (1 mL) and then added dropwise to phosphate-buffered saline (PBS) buffer (10 mL, pH 7.4, 100 mM) under vigorous stirring. The 1,4-dioxane was removed under reduced pressure and the turbid solution was filled up to 10 mL with Milli Q water to maintain the concentration of 1 mg/ml. Determination of the Critical Micelle Concentration (CMC) with Dynamic Light Scattering (DLS) was thereafter investigated according to the literature procedure.[4]

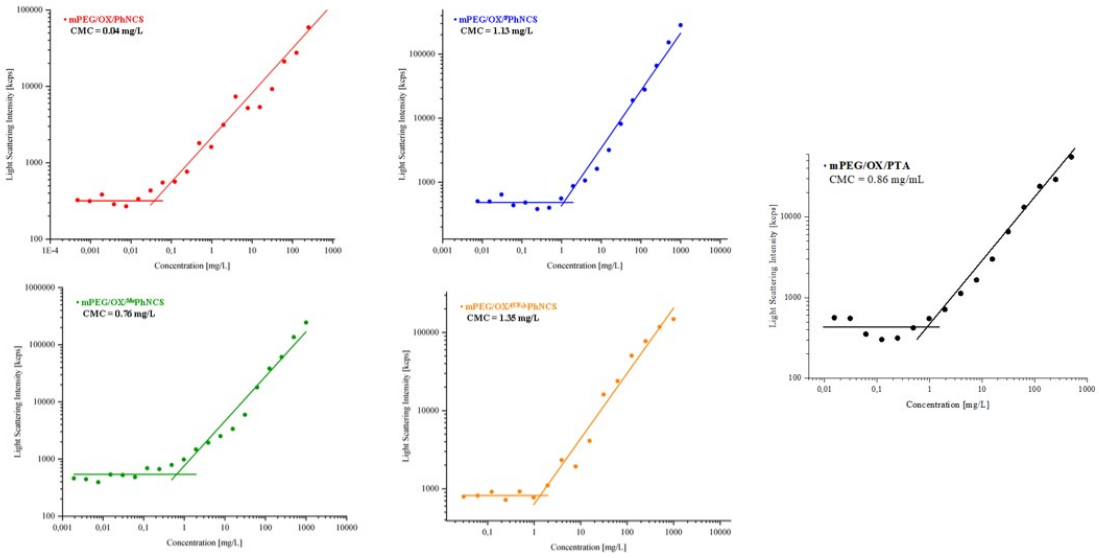

Figure S38: Determination of critical micelle concentration (CMC).

Transition metal coordination

To initially test for the ability of the hydrophobic block to coordinated to transition metal salts, stand-alone copolymer namely OX-co-PhNCS was prepared according to the literature procedure.[3] The polymer (20 mg) was dissolved in $CHCl_3$ and a saturated $(CH_3CN)_2PdCl_2$ solution in CH_3Cl was added dropwise resulting in the immediate precipitation of an orange solid that was isolated by centrifugation and dried in vacuum. Due to its insolubility in all common organic solvents, it was analysed by EDX-coupled SEM confirming the scavenging of $PdCl_2$.

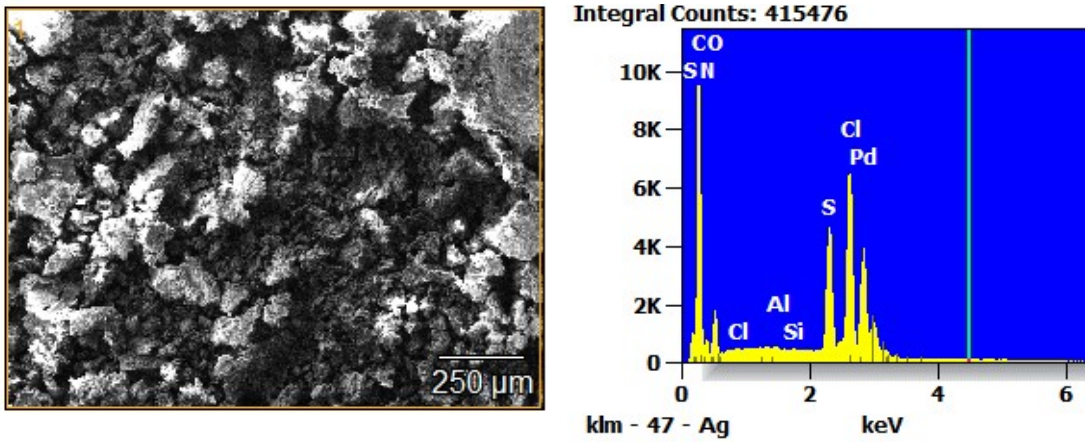

Figure S39: EDX-SEM data for sample prepared as outlined above.

Pd encapsulation: 10 mg of the block copolymer and 20 wt% of $(PhCN)_2PdCl_2$ were dissolved in 1,4-dioxane followed by self-assembly of the mixture via nanoprecipitation by the method outline above. The resulting turbid solutions were passed through a Sephadex G-26 column to separate encapsulated from non-encapsulated materials. The micelle solution was dialysed (1 kDA) against distilled water to remove all organic solvents.

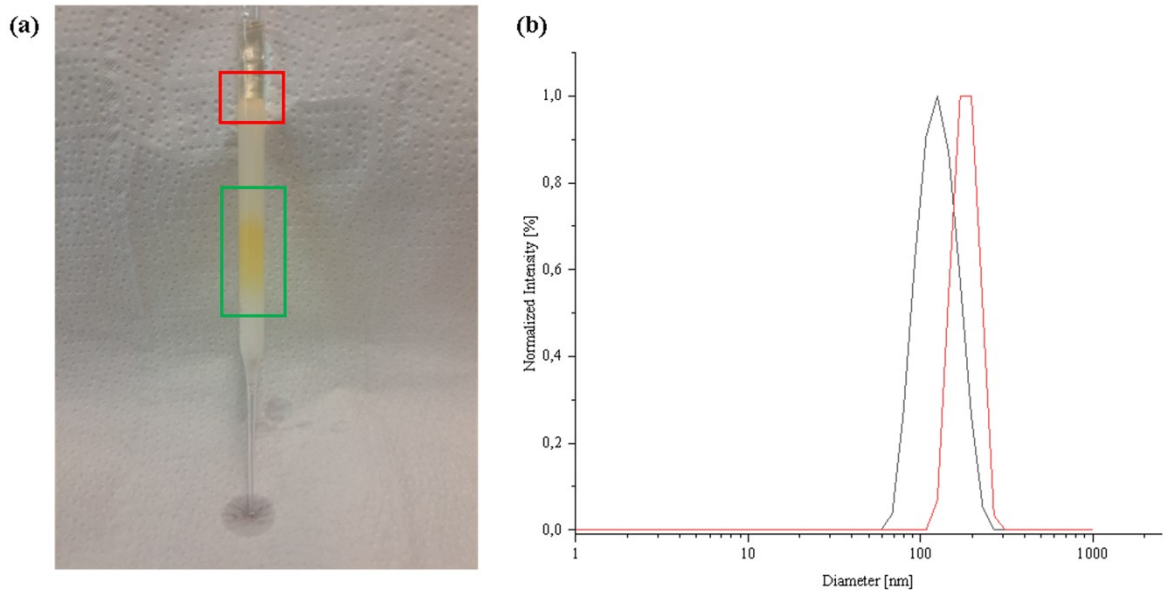

Figure S40: (a) mPEG-*b*-(OX-*co*-PhNCS) micelles encapsulating Pd eluting on the Sephadex G-26 column (green box) with free bis(benzonitrile)palladium(II)chloride residing on top of the column (red box). (b) Comparison of the DLS data (c = 1 mg/mL in PBS Buffer) before (black) and after (red) $PdCl_2$ enapsulation.

Synthesis of *cis*-[Ru(bpy)$_2$(H$_2$O/MeCN)$_2$](BArF)$_2$: NaBArF (183 mg, 0.2 mmol, 1 eq.) was dissolved in 10 mL diethyl ether and added to a solution of $AgNO_3$ (70 mg, 0.4 mmol, 2 eq.) in 5 mL water in a separation funnel wrapped with aluminium foil and shaken vigorously for 5 min. Under light exclusion, the organic phase was separated and transferred into a 20 mL Schlenk tube. The solvent was removed under reduced pressure yielding AgBArF as a white solid which was immediately used.[5] *cis*-[Ru(bpy)$_2$Cl$_2$] (100 mg, 0.2 mmol, 1 eq.) was then dissolved in a 1:1 solution of acetonitrile (5 mL) and water (5 mL) and refluxed at 90 °C for 1.5 h. The hot solution was added to the Schlenk tube containing AgBArF and shaken. The precipitate formed was dissolved by adding 20 mL acetonitrile. Then, the solution was filtered through a 0.2 µm syringe filter and the solvent was removed under reduced pressure yielding cis-[Ru(bpy)$_2$(H$_2$O/MeCN)$_2$](BArF)$_2$ as an orange solid and used for encapsulation within 24 h. Yield: 28 %. ESI-MS *m/z* = calculated: 1359.1604; found: 1359.1813.

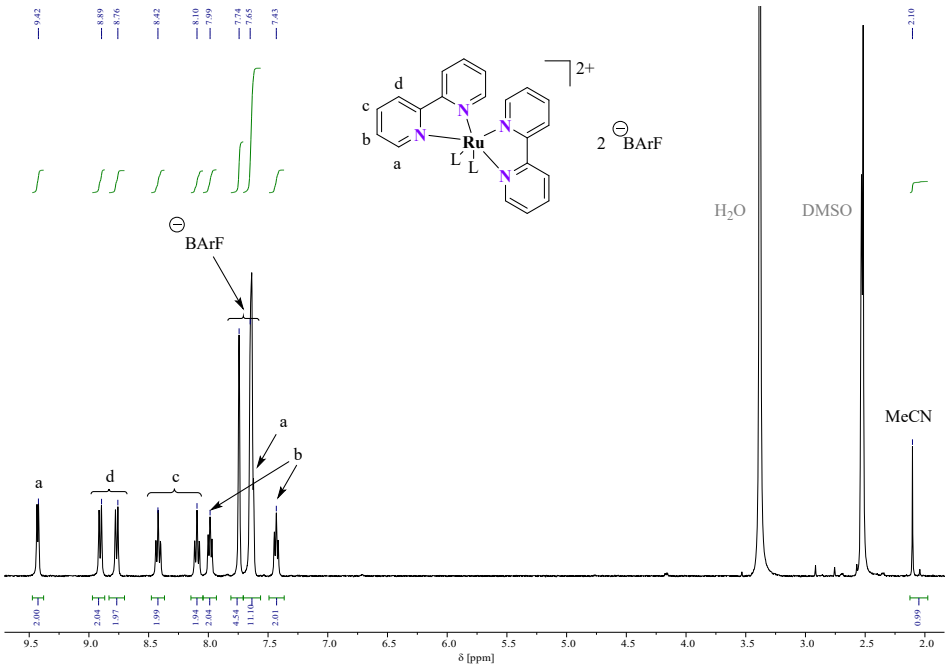

Figure S41: ^{1}H NMR spectrum (400 MHz, DMSO-*d6*, 25°C) of *cis*-[Ru(bpy)$_2$(H$_2$O/MeCN)$_2$](BArF)$_2$.

For ^{1}H NMR analysis, 10 mg of the block polymer and 4 mg of *cis*-[Ru(bpy)$_2$(H$_2$O/MeCN)$_2$](BArF) were dissolved in $CDCl_3$ to control if coordination occurs.

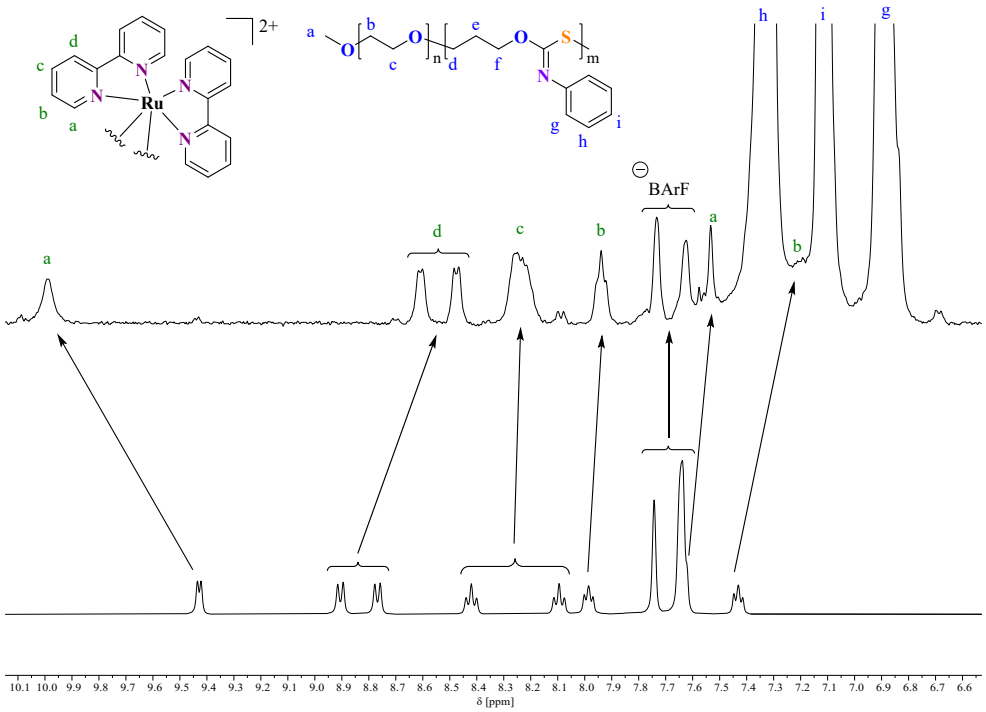

Figure S 42*:* ^{1}H NMR spectrum (400 MHz, $CDCl_3$, 25°C) of block polymer-coordinated *cis*-[Ru(bpy)$_2$(H$_2$O/MeCN)$_2$](BArF)$_2$ in block non-selective solvent. L = H$_2$O/MeCN.

Encapsulation of *cis*-[Ru(bpy)$_2$](BArF)$_2$: 10 mg of the block copolymer and 40 wt% of *cis*-[Ru(bpy)$_2$(H$_2$O/MeCN)$_2$](BArF) were dissolved in a 1:1 mixture of 1,4-dioxane (0.5 mL) and acetonitrile (0.5 mL) followed by self-assembly of the mixture via nanoprecipitation into 10 mL PBS buffer while stirring vigorously. The micelle solution was dialysed (1 kDA) against distilled water to remove all organic solvents.

$^1O_2$ generation: The generation of singlett oxygen was examined after an adapted literature method: A 10 µM (with respect to *cis*-[Ru(bpy)$_2$](BArF)$_2$) micelle solution in PBS buffer was mixed with a 20 µM solution of 9,10-anthracenediyl-bis(methylene)dimalonic acid (ABDA) in water. UV/Vis spectra were recorded before and after every 5 minutes of irradiation (440 nm, 399 mW/cm^2).[6]

References

[1] C. Fornacon-Wood, B. R. Manjunatha, M. R. Stühler, C. Gallizioli, C. Müller, P. Pröhm, A. J. Plajer, *Nat. Commun.* **2023**, *14*, 4525.

[2] C. Fornacon-Wood, M. R. Stühler, C. Gallizioli, B. R. Manjunatha, V. Wachtendorf, B. Schartel, A. J. Plajer, *Chem. Commun.* **2023**, *59*, 11353–11356.

[3] J. Stephan, J. L. Olmedo-Martínez, C. Fornacon-Wood, M. Stühler, M. Dimde, D. Braatz, R. Langer, A. J. Müller, H. Schmalz, A. J. Plajer, *Angew. Chem. Int. Ed.* **2024.**, *63*, e202405047.

[4] D. Braatz, J. H. Peter, M. Dimde, E. Quaas, K. Ludwig, K. Achazi, M. Schirner, M. Ballauff, R. Haag, *J. Mater. Chem. B* **2023**, *11*, 3797–3807.

[5] O. Shyshov, R.-C. Brachvogel, T. Bachmann, R. Srikantharajah, D. Segets, F. Hampel, R. Puchta, M. von Delius, *Angew. Chem. Int. Ed.* **2017**, *56*, 776–781.

[6] H. Wang, Y. Lai, D. Li, J. Karges, P. Zhang, H. Huang, *J. Med. Chem.* **2024**, *67*, 1336–1346.